Research Square

Preprints are preliminary reports that have not undergone peer review.
They should not be considered conclusive, used to inform clinical practice,
or referenced by the media as validated information.

Field-Controlled Modulation Transport in Electro-Optically Accessible Semiconductor Microcavities for Ultrabroadband Optical Interconnects

Babu Dayal Padullaparthi

babudayal@gmail.com

Independent Researcher https://orcid.org/0000-0001-6136-2249

Research Article

Keywords: Microcavity, Modulation, Transport, Vertical-Integgration, VCSEL, Thin Film Niobate, Bandwidth, Ultrabroadband, Photonics

Posted Date: July 22nd, 2026

DOI: https://doi.org/10.21203/rs.3.rs-10424069/v1

License: This work is licensed under a Creative Commons Attribution 4.0 International License.
Read Full License

Additional Declarations: The authors declare no competing interests.

Field-Controlled Modulation Transport in Electro-Optically Accessible Semiconductor Microcavities for Ultrabroadband Optical Interconnects

Babu Dayal Padullaparthi* ***ORCID***
1-1A Hanoi Road, Tsim Shaw Tsui, Kowloon, Hong Kong SAR, PRC
* Email: babudayal@gmail.com,

Abstract

Semiconductor microcavity light sources are fundamentally constrained in modulation speed by carrier–photon dynamics, which impose a relaxation-oscillation bottleneck on bandwidth scaling. Here we introduce an electro-optically integrated vertical-cavity surface-emitting laser platform and a field-controlled modulation transport framework in which cavity accessibility acts as an active transport variable. By integrating thin-film lithium niobate within a GaAs quantum-well VCSEL microcavity, externally applied electric fields directly perturb intracavity optical modes, enabling modulation pathways beyond conventional carrier–photon-limited operation. Physics-based semi-analytical modeling combined with rigorous full-vector 2.5D Maxwell finite-difference time-domain simulations reveals the emergence of three distinct modulation regimes: a conventional carrier–photon-dynamics-limited regime, a hybrid electro-optic–carrier–photon regime, and a transport-dominated regime characterized by suppressed relaxation-oscillation behavior and a quasi-flat ultrabroadband response. The transition is accompanied by systematic cavity-field redistribution while the dominant cavity resonance remains largely preserved, indicating that modulation enhancement originates from field-controlled transport rather than conventional resonance engineering alone. Representative organized modulation transport states exhibit nearly an order-of-magnitude bandwidth enhancement relative to conventional VCSEL operation and follow an approximate scaling with a reduced geometric transport coordinate. These results establish field-controlled modulation transport as a distinct dynamical regime of semiconductor microcavities, providing a framework for understanding EO-assisted modulation beyond conventional relaxation-oscillation limits and a pathway toward sub-terahertz-class photonic transmitters and future high-density optical interconnect systems.

1. Introduction

Semiconductor microcavity lasers (SMLs) employ wavelength-scale optical resonators that confine standing-wave optical fields through distributed Bragg reflector cavities. Their optical behavior is governed by the interplay among cavity quality factor, photon lifetime, intracavity field distribution, carrier transport, and cavity feedback, collectively determining light generation and modulation dynamics [1-3]. Among these, vertical-cavity surface-emitting lasers (VCSELs) represent the most mature and widely deployed SML technology owing to their low threshold current, compact footprint, dense array scalability, wafer-scale manufacturability, and compatibility with advanced photonic integration platforms [4-6]. Their widespread adoption in optical interconnects, sensing systems, datacenter networks, and emerging artificial-intelligence (AI) computing infrastructures has driven sustained efforts to increase modulation bandwidth, energy efficiency, and optical input/output density [7-9]. Despite substantial advances in cavity and photon-lifetime engineering [10], parasitic reduction [11], and coupled-cavity architectures [12-14], the modulation response of conventional VCSELs remains fundamentally governed by coupled carrier–photon dynamics (CPD), which produce the characteristic relaxation-oscillation (RO) response that ultimately limits bandwidth scaling. Although experimental VCSEL bandwidth demonstrations at room temperature have been extended into the 40–50 GHz range through photon–photon resonance, coupled-cavity engineering, and related cavity-assisted modulation mechanisms [15–16], with cryogenic VCSELs further demonstrating record bandwidths exceeding 50 GHz at 2.8 K [17], and enabling transmission beyond 100 GBd [16]; the overall modulation response remains fundamentally rooted in carrier-driven optical dynamics, posing significant challenges for further scaling toward sub-terahertz-class operation. Alternative approaches such as strong optical injection locking in SMLs have demonstrated resonance frequencies exceeding 100 GHz and intrinsic bandwidths approaching 80 GHz by introducing an externally injected optical field that modifies the laser dynamics [18]. However, the requirement for a master laser, precise detuning control, and continuous optical injection has limited widespread deployment in practical optical interconnect systems, motivating exploration of alternative pathways for accessing ultrafast modulation regimes.

In parallel, integrated-photonics platforms employing electro-optic (EO) modulation have demonstrated bandwidths substantially exceeding those attainable in directly modulated SMLs [19-20]. Recent advances in heterogeneous photonic integration, particularly based on thin-film lithium niobate (TFLN), have established a versatile platform for ultrabroadband modulation owing to its large Pockels coefficient ($r_{33} \approx 31$ pm/V), wide transparency window, low optical loss, and compatibility with advanced photonic technologies [21-22]. Despite these advances,

existing descriptions in SML technologies continue to treat the optical cavity as a passive resonator, with modulation governed primarily by CPD and the cavity accessibility remaining largely unexplored as an active transport degree of freedom. Integrating EO-accessible regions directly within a SMLs enables externally applied electric fields to perturb intracavity optical modes and modify their interaction with the gain medium, introducing a cavity-mediated modulation pathway beyond conventional CPD.

Here we investigate a Z-cut TFLN-integrated GaAs quantum-well (QW) VCSEL as a representative EO integrated SML platform, in which cavity accessibility functions as an active transport variable. In this architecture, carrier injection sustains optical generation, while electric-field-induced refractive-index perturbations directly reshape the intracavity optical field through cavity-resonance shifts and effective photon-lifetime modulation. Unlike conventional travelling-wave EO modulators that rely on distributed RF propagation and impedance matching [23], the proposed device operates as a compact lumped EO microcavity in which localized EO perturbations directly modulate the intracavity optical field thereby govern modulation transport. Using hierarchical multiscale modeling that combines physics-based small-signal transport analysis with rigorous full-vector 2.5D Maxwell finite-difference time-domain (FDTD) simulations, we identify three distinct modulation regimes: a conventional CPD-limited regime, a hybrid EO–carrier–photon regime, and a transport-dominated regime characterized by suppressed RO behavior and a quasi-flat ultrabroadband response. The results reveal a systematic transition from resonance-limited modulation to field-controlled modulation transport (FCMT) mediated by cavity accessibility, optical-field redistribution, and EO interaction, establishing a distinct dynamical regime for SML sources beyond conventional CPD-limited operation.

2. Concept and Device Architecture

2.1 EO-Accessible SML Architecture and Modulation Regimes

To investigate the influence of EO cavity accessibility on modulation dynamics, we consider a vertically integrated SML platform in which optical generation and modulation are partially separated through heterogeneous EO integration. In the proposed architecture, carrier injection within the GaAs QW active region sustains optical gain and lasing, while externally applied EO independently perturb the intracavity optical field through an integrated TFLN layer. This configuration introduces a FCMT interaction pathway that operates in parallel with conventional CPD.

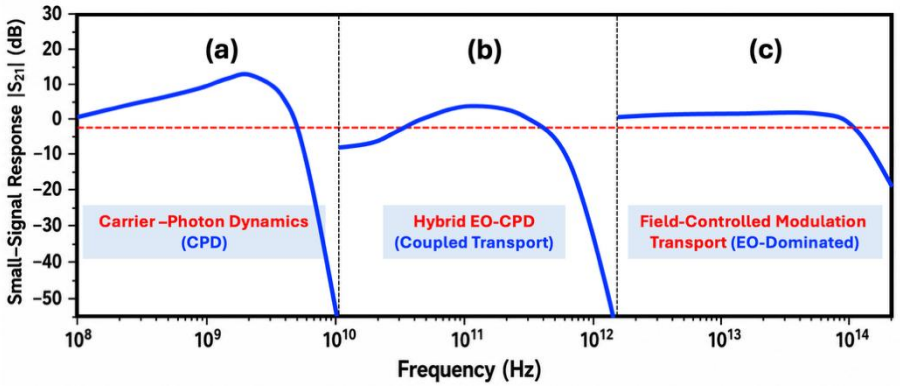


Fig. 1: *Conceptual evolution of modulation transport in EO-integrated semiconductor microcavities. Representative small-signal frequency responses illustrating the transition from (a) conventional carrier–photon dynamics (CPD), through (b) hybrid EO–carrier–photon transport, to (c) organized modulation transport (EO-dominated). The red dashed line denotes the –3 dB bandwidth criterion, illustrating the progressive extension of the modulation bandwidth.*

Figure 1 illustrates the conceptual evolution of modulation transport in EO integrated SMLs. Depending on the degree of EO cavity accessibility and field participation, the small-signal modulation response evolves from (a) conventional CPD, through (b) hybrid EO–CPD coupled transport, to (c) field-controlled modulation transport (FCMT) characterized by progressive suppression of RO behavior and a quasi-flat ultrabroadband frequency response. The red dashed line denotes the −3 dB bandwidth criterion, illustrating the systematic extension of usable modulation bandwidth across the three transport regimes. This evolution suggests that modulation is governed not only by carrier–photon interactions but also by field-controlled cavity accessibility, which provides an additional transport pathway. The resulting transport evolution forms the conceptual foundation of the FCMT framework developed in this work.

2.2 SML and EO states considered

Figure 2 presents the representative SML architectures investigated in this work. Figure 2(a) illustrates a conventional bare VCSEL (BVCL) without EO integration, serving as the reference CPD platform. Figure 2(b) shows the dielectric-mirror EO (DMEO) under intra-cavity contacting (ICC) configuration, in which the integrated TFLN layer is positioned in close proximity to the QW active region, enabling strong EO accessibility and hybrid EO–carrier–photon transport. Figure 2(c) illustrates the optimized EO (OPEO) configuration, where the EO layer is separated from the QWs and interacts predominantly through the intracavity optical field, giving rise to FCMT. Together, these representative architectures provide the physical basis for investigating the transition from conventional CPD to hybrid EO-assisted transport and ultimately to FCMT across the representative cavity states examined in this work

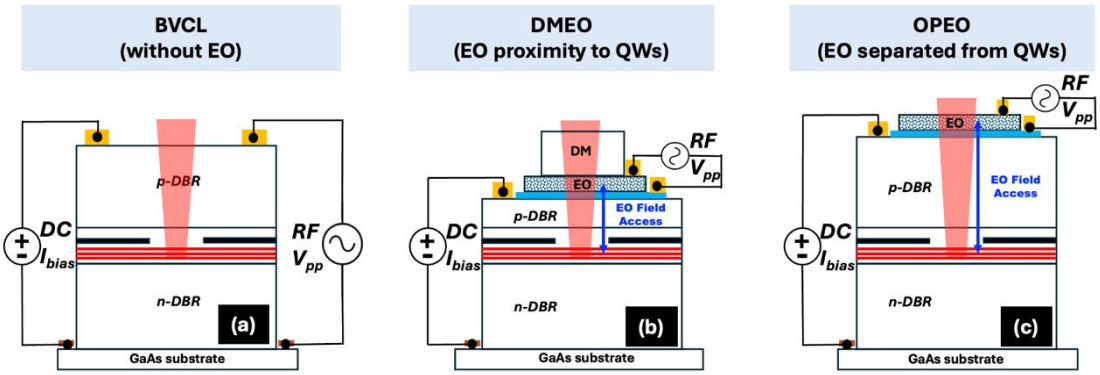


Fig. 2: *Representative semiconductor microcavity architectures illustrating increasing electro-optic (EO) cavity accessibility. (a) Conventional bare VCSEL (BVCL) without EO integration. (b) Dielectric-modulated EO configuration (DMEO), where the EO layer is positioned in close proximity to the quantum-well (QW) active region. (c) Organized passive EO configuration (OPEO), where the EO layer is separated from the QWs while remaining optically accessible through the cavity field. The blue arrows schematically indicate the increasing field-controlled EO accessibility to the active cavity.*

To establish the generalized modulation-transport framework, we investigate the evolution of modulation dynamics as a function of EO cavity accessibility and optical-field participation across three device families: conventional bare VCSELs (BVCL), dielectric-mirror EO microcavities (DMEO), and optimized EO microcavities (OPEO). As each device family comprises multiple cavity configurations or operating states, summarized in Table 1 (Appendix), only a few representative states are presented in the Results to illustrate the progression from CPD to FCMT.

3. Theoretical Framework for FCMT

3.1 Conventional Carrier–Photon Transport (States A1 and B1)

The modulation response of a conventional SML is governed by coupled CPD. Under small-signal excitation, linearization of the carrier and photon rate equations yields the familiar second-order transfer function [3, 10]

$$H_{CPD}(\omega) = \frac{\omega_R^2}{\omega_R^2 - \omega^2 + j\gamma\omega} \qquad (1)$$

where $\omega_R$is the RO frequency and γ is the damping factor. This response describes a resonance-limited transport (shown in Fig.1 (a)) pathway in which carrier populations simultaneously provide optical gain and regulate intracavity photon density. The resulting dynamics produce the characteristic RO peak and high-frequency roll-off that define the modulation bandwidth of conventional VCSELs.

3.2 EO-accessible SMLs

In EO-accessible SMLs, externally applied electric fields directly perturb the optical cavity through the Pockels effect [22, 24-25]. The induced refractive-index variation is

$$\Delta n = -\frac{1}{2} n^3 r_{33} E_{RF} \qquad (2)$$

where n is the refractive index, r_{33} is the EO coefficient, and E_{RF} is the applied RF electric field [21-22, 26]. The corresponding cavity phase perturbation is

$$\Delta\phi = \frac{2\pi}{\lambda} L_{\text{eff}} \Delta n \qquad (3)$$

where L_{eff} is the effective optical interaction length. Unlike conventional VCSELs [3, 10, 24], where modulation is governed by carrier-induced gain variation, the proposed architecture introduces an additional modulation pathway through direct electro-optic perturbation of the intracavity optical mode [19, 27].

3.3 EO-Assisted and EO-Dominated Transport Contribution (States B2 and A2 to A8c)

The EO perturbation also introduces an additional transport pathway that operates alongside conventional CPD. We represent this contribution phenomenologically as

$$H_{EO}(\omega) = \frac{1}{(1+j\omega\tau_{EO})} \qquad (4)$$

where τ_{EO} denotes the effective EO-assisted transport timescale associated with EO perturbation of the intracavity optical field. For $\omega \ll 1/\tau_{EO}$, the EO-assisted pathway responds quasi-statically to the applied modulation, providing an additional field-controlled perturbation that operates alongside conventional CPD. The resulting modulation therefore corresponds to a hybrid EO-assisted transport regime in which both carrier-induced gain modulation and EO-induced cavity perturbation contribute to the overall response. As EO cavity accessibility and field organization increase, the EO-assisted pathway progressively dominates the modulation response, while the relative contribution of conventional CPD diminishes. This transition gives rise to the FCMT regime, characterized by suppression of ROs and a quasi-flat ultrabroadband response. This transfer function does not replace the conventional carrier–photon response but phenomenologically represents the additional field-controlled modulation pathway enabled by EO cavity accessibility, providing the basis for the transition from conventional CPD to FCMT.

3.4 Generalized Modulation Transport

The combined modulation response is therefore governed by the coexistence of carrier-induced gain dynamics and EO-assisted intracavity field perturbation. The overall modulation response may therefore be expressed as

$$H_{total}(\omega) = H_{CPD}(\omega)\, H_{EO}(\omega) \qquad (5)$$

which provides a convenient description of the continuous evolution from conventional resonance-limited modulation (Fig.1 (a)) to ward EO-assisted transport (Fig.1 (b, c)). The relative importance of the two contributions depends on cavity accessibility, EO-field overlap, optical-field organization, and electrodynamic coupling strength. When the EO perturbation is weak, the modulation response remains dominated by conventional CPD and $H_{EO}(\omega) \approx 1$. As EO accessibility increases, the EO-assisted transport pathway begins to contribute alongside the carrier–photon response, with the intracavity optical field inherited from the underlying CPD subsequently undergoing EO-assisted modulation, thereby producing a hybrid EO–CPD regime in which both mechanisms participate simultaneously (Fig. 1(b)) [28-29]. In this intermediate regime, EO-induced cavity perturbation modifies the resonance topology and damping characteristics while carrier-mediated gain modulation continues to govern optical generation. Further increases in EO participation progressively shift the response toward transport-dominated behavior (Fig. 1(c)), where modulation is increasingly determined by FCMT.

4. Results

4.1 Evolution from Resonance-Limited to Transport-Controlled Modulation

The consequences of cavity accessibility become evident in the simulated small-signal modulation response. Figure 3 compares representative frequency responses obtained for conventional BVCL, Pre-DMEO, DMEO and two OPEO states. The conventional VCSEL exhibits the expected second-order response characteristic of coupled CPD, including a pronounced RO peak followed by rapid high-frequency roll-off as shown in Fig. 3(a). This behavior reflects the well-established resonance-limited transport pathway described by conventional laser modulation theory [3, 10, 24].

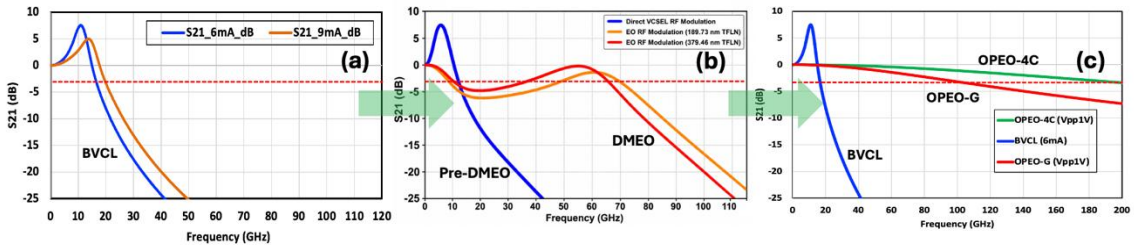


Fig. 3: *Evolution of modulation dynamics in EO-integrated VCSEL microcavities. (a) Simulated |S21| response of a conventional VCSEL (BVCL) exhibiting a characteristic RO resonance associated with underdamped CPD. (b) Coupled EO–CPD regime (DMEO) exhibiting broadened hybrid dynamics and resonance reshaping arising from EO–cavity coupling. (c) EO transport-dominated regime (OPEO) exhibiting suppressed resonance behavior and quasi-flat ultrabroadband response. Green arrows show the modulation transition from (a) to (c).*

The introduction of EO accessibility modifies this response. In the DMEO configuration, modulation broadens beyond the conventional RO-limited response and develops characteristics indicative of simultaneous or hybrid carrier-photon and EO participation as shown in Fig. 3(b). The modulation spectra no longer follows a purely resonance-dominated transfer function but instead exhibits features consistent with coupled transport dynamics involving both cavity-field perturbation and carrier-mediated gain modulation [28-29]. As EO participation increases further, the modulation response evolves toward a transport-dominated state as shown in Fig. 3(c). Representative OPEO-G and OPEO-4C states exhibit progressive suppression of the RO peak and a transition toward a monotonic broadband response, with -3dB modulation bandwidths increasing to 96 GHz and 185 GHz respectively, extending far beyond the bandwidth of the conventional VCSEL cavity. The associated pole evolution qualitatively changes from underdamped complex-conjugate carrier-photon poles to increasingly overdamped transport behavior. These observations indicate a systematic transition from resonance-limited modulation toward transport-controlled dynamics governed by cavity accessibility and EO-assisted field interaction.

An additional feature of Fig. 3 is the progressive reduction in the high-frequency roll-off of the modulation response across the three transport regimes. While the conventional BVCL and hybrid EO–CPD states exhibit the characteristic first-order decay of approximately 20 dB/decade associated with CPD, the field-controlled OPEO states display a substantially flatter response (typically 5–10 dB/decade). The asymptotic high-frequency modulation response may be approximately represented as

$$| H_{Total}(\omega) | \sim \omega^{-\eta} \qquad (6)$$

where η denotes an effective high-frequency decay exponent. For the conventional BVCL and hybrid EO–CPD regimes, $\eta \approx 1$, corresponding to the characteristic first-order roll-off (~20

dB/decade). In contrast, the field-controlled OPEO regime exhibits a substantially smaller effective exponent ($\eta < 1$, approximately 0.25–0.5), corresponding to a much flatter decay (~5–10 dB/decade). The reduction in η provides an additional signature indicates that the modulation transport is progressively governed by the EO-assisted intracavity field rather than solely by CPD, providing further evidence for the transition to FCMT.

4.2 Electrodynamic Evolution of EO-Accessible Microcavities

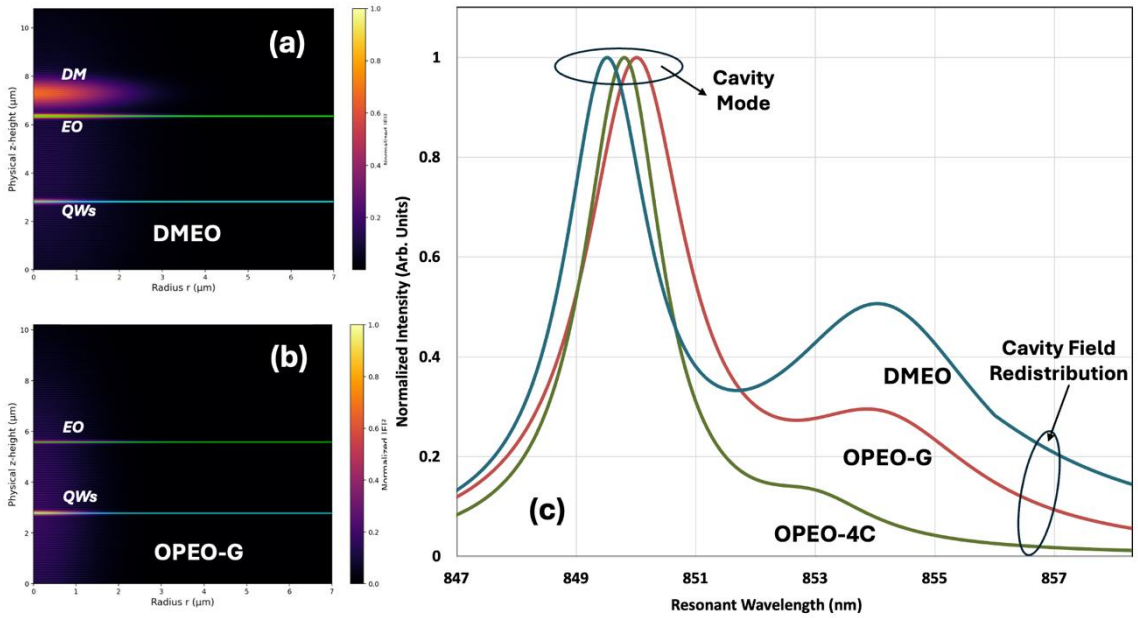


Fig. 4: *Electrodynamic evolution of EO-integrated VCSEL microcavities obtained from full-vector 2.5D Maxwell–FDTD simulations. (a, b) Two-dimensional normalized electric-field distributions for representative DMEO and OPEO-G configurations and (c) Overlaid normalized resonance spectra for states DMEO (B2), OPEO-G(A2) and OPEO-4C (A8c). Horizontal lines in (a) and (b) representing field monitors in FDTD.*

Rigorous 2.5D Maxwell-FDTD simulations in Fig. 4 were performed for all states in Table-1 to visualize the underlying electrodynamic field redistribution induced by EO integration inside the microcavity. Relative to the BVCL (A1, not shown here), the EO-integrated architectures (DMEO and OPEO-G) in Fig. 4(a, b) progressively redistribute the standing-wave field toward the dielectric EO region while maintaining strong confinement within the active semiconductor cavity [30]. The resulting hybrid semiconductor–dielectric cavity interaction establishes finite EO-accessible optical participation without disrupting active-region confinement, enabling the transition from conventional CPD modulation toward EO-assisted transport dynamics and FCMT. This electrodynamic evolution is further reflected in the resonance spectra of Fig. 4(c), where the systematic emergence of long-wavelength spectral redistribution from DMEO to OPEO-4C indicates increasing cavity-phase perturbation, photon-lifetime reorganization, and hybrid EO-assisted cavity transport (refer Table-1). The associated resonance perturbation and

spectral reshaping are conceptually analogous resonance-shift and coupled-cavity spectral-evolution phenomena previously reported in integrated micro-resonator photonic systems [31].

A notable observation from Fig. 4(c), is that the primary cavity resonance remains centered near 850 nm across all configurations despite substantial differences in modulation bandwidth. The preservation of the principal cavity mode indicates that transport enhancement does not arise from simple resonance shifting or cavity broadening. Instead, the dominant changes occur within a secondary long-wavelength spectral component that evolves systematically across the OPEO states. Thus, the OPEO states shown in Fig. 3 and Fig. 4 together describe not only the progressive transition from conventional CPD-limited modulation toward hybrid EO-assisted and transport-dominated electrodynamic cavity behaviour, but also extending earlier concepts of gain and cavity-Q modulation proposed by Iga [32].

4.3 Emergence of Organized Modulation Transport States

To investigate the origin of transport enhancement, we examine representative EO-accessible transport states spanning hybrid and organized modulation transport regimes. Figure 5 compares the transverse optical-field distributions within the TFLN layer for the DMEO, OPEO-G, and OPEO-4C configurations. The DMEO state exhibits broad optical participation throughout the EO-accessible region, consistent with strong cavity-field redistribution and hybrid EO–carrier–photon transport. OPEO-G represents an intermediate organized transport state with increased field concentration while maintaining substantial EO accessibility. In contrast, OPEO-4C exhibits pronounced field localization within the EO-accessible region, indicating a highly organized transport state. The observed progression from broad field participation to localized confinement suggests that modulation transport enhancement is accompanied by systematic cavity-field organization rather than large changes in the fundamental cavity resonance.

The simultaneous evolution of resonance structure (Fig. 4(c)) and cavity-field organization (Fig. 5) suggests that modulation enhancement originates from redistribution of optical participation within the EO-accessible microcavity. We therefore interpret these states as organized modulation transport states, in which cavity accessibility, optical confinement, and EO interaction collectively determine the transport response. Unlike conventional carrier-photon transport, which is governed primarily by gain and photon storage, the organized states emerge through coordinated cavity-field participation across coupled semiconductor and EO regions.

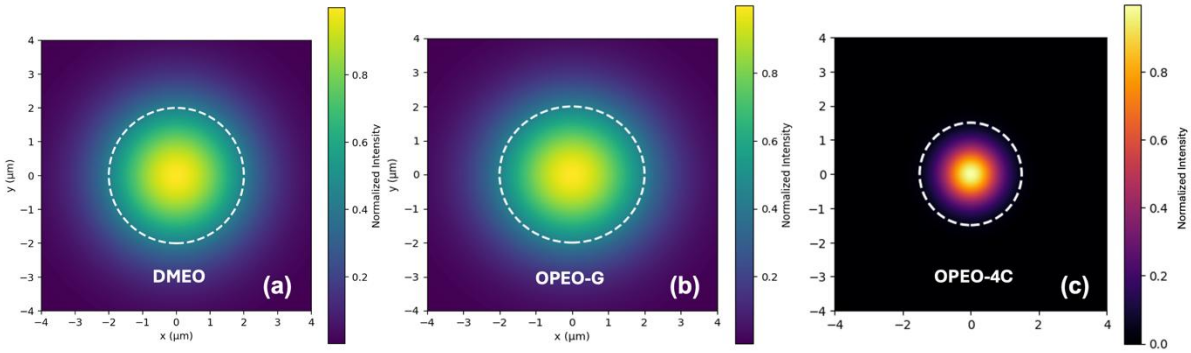


Fig. 5: *Evolution of normalized transverse optical-field distributions within the TFLN layer from full-vector 2.5D Maxwell–FDTD simulations for representative organized modulation transport states (a) DEMO, (b) OPEO-G, and (c) OPEO-4C. The dashed circle denotes the EO-accessible region.*

4.4 Transport States Organization

The organization of the representative OPEO states suggests that modulation transport is governed not by any single structural parameter, but by collective cavity-field dynamics. In EO-integrated semiconductor microcavities, the optical field is determined by the cavity eigenvalue problem

$$\nabla \times \nabla \times E = \frac{\omega^2}{c^2}\varepsilon(\mathbf{r})E \qquad (7)$$

where $\varepsilon(\mathbf{r})$describes the spatial dielectric distribution of the coupled semiconductor–electro-optic cavity [2, 33]. Consequently, modifications to EO accessibility, optical confinement, and cavity geometry collectively reorganize the intracavity field distribution and thereby influence modulation transport. To parameterize the observed transport evolution, we introduce a reduced geometric transport coordinate

$$\Lambda \approx \frac{t_{SiN}}{D_{EO}t_{EO}} \qquad (8)$$

where D_{EO}, t_{EO}, and t_{SiN}denote the EO diameter, EO thickness, and SiN thickness, respectively. The coordinate Λ combines the principal geometric variables governing optical confinement, EO accessibility, and cavity participation, while remaining consistent with practical fabrication constraints and minimum realizable feature dimensions. Although empirical in form, Λ provides a compact descriptor of the cavity geometries explored in this work and captures the competing influences of optical confinement, EO accessibility, and cavity participation. Such behaviour is reminiscent of emergent order parameters and modal organization in open photonic systems, where large numbers of microscopic degrees of freedom become represented by a smaller set of collective observables [34].

The representative OPEO states exhibit an approximate power-law relationship between modulation bandwidth and the reduced transport coordinate,

$$f_{-3dB}(Bandwidth) \propto \Lambda^{0.4} \quad (9)$$

indicating that modulation transport evolves systematically with cavity-field organization. While the present relation is empirical and derived from a limited set of representative states, the observed scaling suggests that EO-enhanced modulation is governed by collective geometric and electrodynamic interactions rather than by individual structural parameters considered independently. The resulting behavior supports the interpretation of organized modulation transport as an emergent consequence of cavity-field redistribution within EO-accessible SMLs. Further extrapolation of the present OPEO design space suggests that, for the investigated TFLN-SiN geometries and practical RF engineering constraints, modulation bandwidths approaching 250 GHz may be attainable. This value should therefore be regarded as an engineering-guided upper bound for the present device architecture rather than a fundamental physical limit. A comprehensive transport-state analysis encompassing the full OPEO design space will be presented in future work.

5. Discussion

5.1 Beyond Conventional Carrier–Photon Modulation

The results demonstrate that modulation transport in EO accessible SMLs extends beyond conventional CPD. While modulation in traditional semiconductor lasers is governed by coupled carrier–photon interactions that produce RO-limited responses, the EO-integrated microcavities investigated here exhibit systematic cavity-field redistribution and reorganization of optical participation while preserving the dominant cavity resonance. The observed modulation enhancement therefore cannot be explained solely by resonance broadening or cavity-frequency shifts, but instead indicates the emergence of an additional cavity-mediated transport pathway enabled by direct EO access to the intracavity field. As EO participation increases, modulation evolves from a CPD process toward FCMT characterized by progressively suppressed RO and broadband response, suggesting a transition in modulation dynamics rather than a conventional bandwidth-enhancement mechanism.

5.2 Organized Modulation Transport States and FCMT

A central observation of this work is the emergence of organized modulation transport states arising from collective reorganization of cavity accessibility, optical confinement, and electro-

optic participation. The resonance and field-distribution results show that transport enhancement is accompanied by systematic redistribution of optical participation within the EO-accessible cavity while preserving the dominant cavity mode, indicating that the observed transport hierarchy reflects organized electrodynamic states rather than independent device optimizations. These findings suggest that EO accessibility functions as an organizing variable linking cavity-field redistribution, optical confinement, and modulation dynamics, transforming the microcavity from a passive resonator into an active participant in modulation transport.

5.3 Generality of the Framework

Although a TFLN-integrated 850-nm GaAs quantum-well VCSEL platform is demonstrated here, the underlying transport concept is not limited to a specific material system or device architecture. More generally, any active photonic microcavity combining optical gain with an externally accessible cavity region may support FCMT. Consequently, similar behavior may emerge in strained QW lasers, quantum-dot lasers, coupled semiconductor resonators, dielectric microcavities, and heterogeneous photonic platforms incorporating EO materials such as lithium niobate (LN or $LiNbO_3$), lithium tantalate (LT or $LiTaO_3$), EO polymers, or related active Pockel's media. These results suggest that cavity accessibility may serve as a general organizing principle for modulation transport beyond conventional carrier–photon-limited operation.

6. Conclusions

We have introduced a field-controlled modulation transport (FCMT) framework for electro-optically (EO) accessible semiconductor microcavity lasers (SMLs) and demonstrated its emergence using a thin-film lithium niobate (TFLN) integrated VCSEL platform. Combining generalized transport analysis with full-vector electrodynamic simulations, we identified a progression from conventional carrier–photon-dominated (CPD) modulation to hybrid EO–carrier–photon transport and organized modulation transport states. The results show that EO cavity accessibility drives systematic redistribution of optical participation and cavity-field organization while largely preserving the fundamental cavity resonance. This evolution is accompanied by suppression of relaxation-oscillation (RO) behavior and a transition from resonance-limited to transport-controlled modulation responses with substantially enhanced bandwidths to sub-THz regime. The observed enhancement originates from collective reorganization of optical confinement, EO accessibility, and cavity participation rather than from conventional resonance engineering alone. These findings establish cavity accessibility as

an active transport variable and identify FCMT as a distinct dynamical regime of SMLs. More broadly, the framework may extend to a wide range of EO-integrated photonic resonators and provide new opportunities for engineering ultrabroadband photonic transmitters and future high-density optical interconnect systems.

7. Online Methods

7.1 Representative Semiconductor Microcavity Platform

A representative 850 nm GaAs QW VCSEL incorporating an integrated Z-cut TFLN EO layer was employed as the reference platform throughout this study. The baseline VCSEL comprised p-type and n-type $Al_xGa_{1-x}As$ (x = 0.15-0.85) DBRs incorporating 20 nm graded-index transition layers, together with a SiO_2/Ta_2O_5 dielectric mirror surrounding a one-wavelength active cavity containing three GaAs QWs and supporting the fundamental longitudinal mode near 850 nm. Unless otherwise specified, the n-DBR and p-DBR contained fixed mirror pair numbers of 34 and 21, respectively, with mesa diameters of 60 μm (n-side) and 30 μm (p-side), a 6 μm oxide aperture, for all modeled device states. The electrical model employed a fixed series resistance of 60 Ω together with the differential gain, transparency carrier density, and gain-compression parameters adopted from Ref. 11. For the CPD model, the D-factor was fixed at 5.0 GHz $mA^{-1/2}$, while a K-factor of 0.3 ns was used for the BVCL and Pre-DMEO reference structures. Relevant parameters are summarized in Supplementary Table 1**.**

7.2 EO Integration Framework

EO cavity accessibility was introduced by integrating a Z-cut TFLN–SiN stack within the optical cavity, enabling externally applied electric fields to directly perturb the standing-wave intracavity optical mode while preserving optical generation within the semiconductor active region. The SiN aperture (14 μm diameter) was fixed for all EO-integrated device configurations except the Bare VCSEL (BVCL) and Pre-DMEO reference structures. For all EO-integrated states, the EO aperture diameter, EO layer thickness, and SiN thickness were treated as independent design variables, whereas all remaining VCSEL structural and material parameters were held constant. This parameterization isolated the influence of cavity accessibility on FCMT while maintaining a common semiconductor laser platform across all modeled states. Although the present study focuses on a GaAs QW VCSEL platform, preliminary simulations performed using equivalent strained InGaAs QWs predict further enhancement of modulation bandwidth, indicating that the FCMT framework is not restricted to a specific gain medium and is expected to extend to a broader class of EO-integrated semiconductor microcavity lasers (SMLs).

7.3 Multiscale Modeling Framework

The study employed a hierarchical multiscale physics-based semi-analytical and numerical modeling framework combining transfer-matrix method analysis, full-vector electrodynamic simulations, transport modeling, and modulation-response analysis. Transfer-matrix calculations were used to establish cavity resonance conditions, optical confinement, and photon-lifetime characteristics of the EO-integrated microcavities, while rigorous 2.5D Maxwell FDTD simulations were performed to evaluate resonance evolution, intracavity-field redistribution, and optical participation within the EO-accessible region. Modulation dynamics were subsequently analyzed using a generalized small-signal framework incorporating both carrier–photon and EO-assisted transport pathways. This integrated workflow enabled consistent investigation of conventional VCSEL, hybrid EO-integrated, and transport-dominated cavity configurations within a unified modeling framework.

7.4 Electrodynamic Simulations

Rigorous full-vector 2.5D Maxwell FDTD simulations were performed using a custom-developed solver with CW Gaussian beam to investigate optical confinement, cavity-field redistribution, resonance evolution, and electro-optic participation in the integrated microcavity structures [35-36]. The simulations incorporated realistic dielectric material properties, DBR reflectivities, cavity geometries, and optical boundary conditions across representative conventional VCSEL, EO-integrated, and organized transport states. Quantities extracted included longitudinal and transverse optical-field distributions, optical confinement factors, photon lifetimes, resonance spectra, and EO-accessible optical participation are given Table-1. These results were used to establish the relationship between cavity accessibility, field organization, and modulation transport in EO-integrated semiconductor microcavities.

7.5 Small-Signal Modulation Analysis

Small-signal frequency responses were evaluated over a broad frequency range for representative cavity configurations spanning conventional VCSEL operation, hybrid EO–carrier–photon transport states, and organized modulation transport states [14, 24-25]. Modulation behavior was examined as a function of EO-layer thickness, EO diameter, dielectric confinement thickness through the reduced transport coordinate (Λ) (see Table-1), cavity topology, and EO–QW interaction strength, with emphasis on the evolution of relaxation-oscillation behavior, resonance topology, modulation bandwidth, and transport-regime transitions. Bandwidth enhancement, spectral redistribution, and transport evolution were

evaluated consistently across all simulated structures to establish the modulation-regime hierarchy reported in results section.

Appendix:

Table 1: Electrodynamic Characteristics and Modulation Performance of Representative EO-Accessible Microcavity States*

Configuration	p-DBR (Pairs)	Dielectric Mirror (Pairs)	Transport Coordinate Λ (cm-1)	Γ_{QW} (%)	$\Gamma_{TFLN/DM}$ (%)	EO Field Participation Factor	Resonance Wavelength (nm)	Resonance Shift (nm)	Photon Lifetime τ_p (ps)	Cavity Quality Factor Q	S21 Bandwidth (GHz)	Operational State
Bare VCSEL (A1)	21	0	N/A	6.42	0.00*	0.08	849.9	~0.01	7.6	1580	16	BVCL
EO+VCSEL (A2)	21	0	0.141	5.18	1.34	0.25	849.7	0.11	5.9	1210	96	OPEO-G
EO+VCSEL (A3)	21	0	0.189	5.35	1.05	0.19	849.7	0.08	6.3	1290	105	OPEO-1
EO+VCSEL (A4)	21	0	0.566	5.62	0.72	0.12	849.75	0.05	6.8	1380	120	OPEO-2
EO+VCSEL (A5)	21	0	0.283	5.48	0.92	0.17	849.72	0.07	6.4	1320	112	OPEO-2A
EO+VCSEL (A6)	21	0	0.566	5.58	0.84	0.15	849.78	0.05	6.7	1360	145	OPEO-2B
EO+VCSEL (A7c)	21	0	0.283	5.2	1.48	0.28	849.66	0.14	5.8	1180	120	OPEO-3C
EO+VCSEL (A7d)	21	0	0.849	5.72	0.96	0.17	849.78	0.06	6.7	1360	180	OPEO-3D
EO+VCSEL (A8c)	21	0	0.755	5.78	0.52	0.09	849.84	0.03	7.2	1480	185	OPEO-4C
VCSEL+DM (ICC) (B1)	4	7	N/A	5.34	2.18	0.46	849.7	0.05	5.4	1120	15	Pre-DMEO
VCSEL+DM +EO (ICC) (B2)	4	7	0.023	4.62	3.88	0.71	849.5	0.32	4.1	860	60	DMEO

* Transport Co-ordinate $\Lambda = \frac{t_{SiN}}{D_{EO}\, t_{EO}}$ $(\mu m)^{-1}$ for A2-A8c and B2

Acknowledgements

The author gratefully acknowledges Prof. Kenichi Iga for valuable discussions on semiconductor-laser modulation mechanisms and for drawing attention to early studies on gain and cavity-Q modulation, which helped place the present work within a broader historical context. The author also acknowledges Prof. Dieter Bimberg for insightful discussions, constructive feedback, and encouragement regarding the broader significance and positioning of this work, and Dr. Nim Kwan Cheung for valuable discussions and encouragement during its development stage. The author further acknowledges Dr. Sanjukta Ghosh for logistical support and encouragement that facilitated the completion of this work.

Author Contributions

The author conceived the idea, developed the theoretical framework and analytical model, performed all derivations and analyses, interpreted the results, prepared the figures, and wrote the manuscript.

References

1. Yamamoto, Y. & Slusher, R. E. Optical processes in microcavities. *Phys. Today* **46**, 66–73 (1993).
2. Kavokin, A. V., Baumberg, J. J., Malpuech, G. & Laussy, F. P. *Microcavities*. 2nd edn (Oxford University Press, 2017).
3. Coldren, L. A. & Corzine, S. W. *Diode Lasers and Photonic Integrated Circuits* (Wiley, 1995).
4. Iga, K. Vertical-cavity surface-emitting laser: its conception and evolution. *Jpn. J. Appl. Phys.* **47**, 1–10 (2008).
5. Padullaparthi, B. D., Tatum, J. A. & Iga, K. *VCSEL Industry: Communication and Sensing.* (Wiley-IEEE Press, Hoboken, NJ, 2022).
6. Pan, G. *et al.* Harnessing the capabilities of VCSELs: unlocking the potential for advanced integrated photonic devices and systems. *Light Sci. Appl.* **13**, 229 (2024).
7. Miller, D. A. B. Attojoule optoelectronics for low-energy information processing and communications. *J. Lightwave Technol.* 35, 346–396 (2017).
8. Kohli, M. & Teissier, J. VCSEL-based CPO for scale-up in AI datacenters: status and perspectives. *arXiv* 2601.14342 (2026). https://doi.org/10.48550/arXiv.2601.14342
9. Winzer, P. J. The future of communications is massively parallel. *J. Opt. Commun. Netw.* **15**, 783–790 (2023).
10. Larsson, A. Advances in VCSELs for communication and sensing. *IEEE J. Sel. Top. Quantum Electron.* **17**, 1552–1567 (2011).
11. Westbergh, P. et al. High-speed oxide confined 850 nm VCSELs. *IEEE Journal of Selected Topics in Quantum Electronics* **17**, 1603–1613 (2011).
12. North, W. *et al.* Analysis and characterization of photon–photon resonance in coupled dual-element photonic crystal VCSEL arrays. *J. Lightwave Technol.* **41**, 6638–6645 (2023).
13. Heidari, E. *et al.* VCSEL with multi-transverse cavities with bandwidth beyond 100 GHz. *Nanophotonics* **10**, 3779–3788 (2021).
14. Germann, T. D. *et al.* Electro-optical resonance modulation of vertical-cavity surface-emitting lasers. *Opt. Express* **20**, 5099–5113 (2012).
15. Padullaparthi, B. D. *et al.* Over 39 GHz-bandwidth of directly modulated 1060 nm single-mode VCSEL with intra-cavity metal aperture. In *Conference on Lasers and Electro Optics*, STu3C.3 (2024).
16. Ibrahim, H. R. *et al.* 200-Gb/s 1060-nm single-mode coupled-cavity VCSEL enabling modal-dispersion-free >50-GHz operation. In *Optical Fiber Communication Conference (OFC) 2026*, W4E.3 (2026).
17. Wu, H. et al. Cryogenic oxide-VCSEL at 2.8 K demonstrates record bandwidth $f_{-3\mathrm{dB}}$>50 GHz, P_{out}>14 mW and PAM-4 data rate up to 128 Gb/s. In *Optical Fiber Communication Conference (OFC)*, M3F.4 (2024).
18. Lau, E. K., Zhao, X., Sung, H.-K., Parekh, D., Chang-Hasnain, C. & Wu, M. C. Strong optical injection-locked semiconductor lasers demonstrating >100-GHz resonance frequencies and 80-GHz intrinsic bandwidths. *Opt. Express* **16**, 6609–6618 (2008).
19. Wang, C. *et al.* Integrated lithium niobate electro-optic modulators operating at CMOS-compatible voltages. *Nature* **562**, 101–104 (2018).
20. Komljenovic, T. *et al.* Heterogeneous silicon photonic integrated circuits. *J. Lightwave Technol.* **34**, 20–35 (2016).
21. Zhang, Y. *et al.* Photonic multimode modulation and integrated photonic architectures for next-generation optical interconnects. *Light Sci. Appl.* **11**, 45 (2022).
22. Zhu, D. *et al.* Integrated photonics on thin-film lithium niobate. *Adv. Opt. Photonics* **13**, 242–352 (2021).
23. Leuthold, J. *et al.* High-speed, low-power optical modulators in silicon. In *15th International Conference on Transparent Optical Networks (ICTON)*, We.D2.1 (2013).
24. Agrawal, G. P. & Dutta, N. K. *Semiconductor Lasers*, 2nd edn (Springer, 1993).

25. Saleh, B. E. A. & Teich, M. C. *Fundamentals of Photonics*, 3rd edn (Wiley, 2019).
26. Reed, G. T. *et al.* Silicon optical modulators. *Nat. Photonics* **4**, 518–526 (2010).
27. Xu, M., He, M., Zhang, H. *et al.* High-performance coherent optical modulators based on thin-film lithium niobate platform. *Nat Commun* **11**, 3911 (2020).
28. Haus, H. A. *Waves and Fields in Optoelectronics* (Prentice Hall, 1984).
29. Suh, W., Wang, Z. & Fan, S. Temporal coupled-mode theory and the presence of non-orthogonal modes in lossless multimode cavities. *IEEE J. Quantum Electron.* **40**, 1511–1518 (2004).
30. Bienstman, P. & Baets, R. Optical modelling of photonic crystals and VCSELs using eigenmode expansion and perfectly matched layers. *Opt. Quantum Electron.* **33**, 327–341 (2001).
31. Xu, Q. *et al.* Experimental realization of an on-chip all-optical analogue to electromagnetically induced transparency. *Phys. Rev. Lett.* **96**, 123901 (2006).
32. Iga, K. Modulation limit of semiconductor lasers by some parametric modulation schemes. *Trans. Inst. Electron. Commun. Eng. Jpn. E* **68**, 417–420 (1985).
33. Joannopoulos, J. D., Johnson, S. G., Winn, J. N. & Meade, R. D. *Photonic Crystals: Molding the Flow of Light*, 2nd edn (Princeton Univ. Press, 2008).
34. Haken, H. *Light: Laser Light Dynamics*, Vol. 2 (North-Holland, 1985).
35. Piprek, J. *Semiconductor Optoelectronic Devices: Introduction to Physics and Simulation* (Academic Press, 2003).
36. Taflove, A. & Hagness, S. C. *Computational Electrodynamics: The Finite-Difference Time-Domain Method*, 3rd edn (Artech House, 2005).